Geochemical Perspectives Letters

Tight bounds on missing late veneer in early Archean peridotite from triple oxygen isotopes

S.T.M. Peters, M.B. Fischer, A. Pack, K. Szilas, P.W.U. Appel, C. Münker, L. Dallai, C.S. Marien

Supplementary Information

The Supplementary Information includes:

S-1. Sample Suite

We determined the triple oxygen isotope compositions of olivine from a suite of post-Archean, off-cratonic spinel lherzolite xenoliths, with the exceptions of samples from Hawaii and Beni Boussera, which are dunites. The majority of samples were erupted in continental intraplate magmas, with some samples having erupted in continental rift settings. We studied xenoliths from the East-African Rift system (Great Rift Valley, Ethiopia), the European Cenozoic Rift System (French Massif Central, West Eifel, Hessian Graben, Vogelsberg volcanic field, Ohře/Eger Graben), the Rio Grande Rift (Potrillo Volcanic Field, USA), the Middle Atlas mountains, (Tafraout maar, Morocco), the West Antarctic Rift (Mt. Melbourne volcanic field), and the Eastern block of the North China craton (Changle volcano). In order to investigate whether $\Delta'^{17}O$ values of

subcontinental lithospheric mantle peridotite could potentially have been affected by metasomatic processes or processes of re-fertilisation, we also determined the triple oxygen isotope composition of a peridotite xenolith from the Dariganga volcanic plateau, Mongolia (sample 8520-12), that was previously reported to have a $\delta^{18}O_{ol}$ value of 5.50 ± 0.09 ‰ (Wiechert *et al.*, 1997), *i.e.* a higher $\delta^{18}O_{ol}$ value than typical mantle peridotite ($\delta^{18}O_{ol} \approx 5.2$ ‰). We did not reproduce the elevated $\delta^{18}O_{ol}$ value for this sample, and measured a $\delta^{18}O_{ol}$ of 5.15 ± 0.06 ‰ (Table S-1). A sample of orogenic peridotite from the Beni Boussera lherzolite massif in Morocco (14BB2) was included in the sample suite well. Samples from the suboceanic lithospheric mantle were also measured, and include peridotite xenoliths that were erupted in ocean island basalts (OIBs) from Hawaii (Hualālai volcano), Lanzarote, and Tenerife.

We then determined the triple oxygen isotope compositions of olivine in Archean peridotite, predominantly of dunite composition, from the ultramafic enclaves in the Itsaq Gneiss Complex (IGC) and Fiskefjord region of southwest Greenland. We studied peridotite samples from two localities in the >3.7 Ga Isua supracrustal belt (ISB) (Dymek *et al.*, 1988; Friend *et al.*, 2002; Friend and Nutman, 2011), one locality south of the Isua supracrustal belt (SOISB; Bennett *et al.*, 2002; Friend *et al.*, 2002; van de Löcht *et al.*, 2020), the ~3.8 Ga Narssaq ultramafic body (NUB; Nutman *et al.*, 2007; van de Löcht *et al.*, 2020), and the ~3.8 Ga Ujaragssuit Nunât ultramafic body (Rollinson, 2002; Lowry *et al.*, 2003). Each of these ultramafic enclaves carries an s-process Ru excess compared to the BSE (Fischer-Gödde *et al.*, 2020). The samples from SOISB (10-27, 10-28) and one sample from NUB (10-09) that were analysed in the present study are aliquots of the same samples for which Fischer-Gödde *et al.* (2020) also reported s-process excess Ru. The petrogenesis of these particular samples is discussed in detail by van de Löcht *et al.* (2020). We also determined the triple oxygen isotope compositions of olivine from ultramafic enclaves in the Mesoarchean Fiskefjord region that are geologically related to the Seqi peridotite body (Szilas *et al.*, 2015a), for which excess s-process Ru compared to the bulk silicate Earth was also reported (Fischer-Gödde *et al.*, 2020). Most of the ultramafic enclaves that were studied have been interpreted as slivers of residual mantle peridotite that were entrained in

the Archean crust (Nutman *et al.*, 1996; Bennett *et al.*, 2002; Friend *et al.*, 2002; Rollinson, 2007; van de Löcht *et al.*, 2018, 2020) or, alternatively, as cumulates from (ultra)mafic magmas (*e.g.*, Dymek *et al.*, 1988; Frei *et al.*, 2004; Szilas *et al.*, 2015a, 2015b). The Ujaragssuit Nunât ultramafic body was interpreted as a layered intrusion with intact magmatic layering (Rollinson, 2002).

A common feature of the ultramafic enclaves from the IGC and Fiskefjord region is that forsterite contents in olivine can range up to comparatively high values, with forsterite contents up to 98 mol% reported in samples from the ultramafic lenses of Isua (Friend and Nutman, 2011). Magnetite is often present in the peridotite samples as well, and in some cases the presence of Ti-clinohumite has been reported (Dymek *et al.*, 1988; Friend and Nutman, 2011). These features are in notable agreement with our interpretation that some olivine in the ultramafic enclaves possibly formed by the dehydration of serpentinite minerals (Nishio *et al.*, 2019; Peters *et al.*, 2020). For 3 samples from SOIB and NUB this interpretation is also in line with disturbed internal ^{87}Rb-^{87}Sr and ^{147}Sm-^{143}Nd isochrons, which suggest multiple overprints by fluids for these particular samples (van de Löcht, 2019).

S-2. Analytical Methods

Hand specimens of rock samples were crushed and sieved in different grain size fractions, such that inclusion-free, alteration-free olivine grains could be hand-picked under a binocular microscope for analysis. The samples were reacted with excess BrF_5 in a stainless-steel sample chamber at a pressure of *ca*. 120 mbar, using a laser for heating of the samples. The equivalent sample mass of ~30 μmol O_2 (*i.e.* 2.0–2.2 mg olivine) was reacted, meaning that a single extraction of O_2 typically comprised one to four olivine grains for samples of mantle peridotite xenoliths and five to ten olivine grains for samples of the Archean ultramafic enclaves in southwest Greenland. The O_2 that was released from the samples was cleaned from contaminant gases in a vacuum line using liquid nitrogen-based cooling techniques, NaCl, and a Hewlett Packard 5890 Series II gas chromatograph at 50 °C (Pack *et al.*, 2016; Peters *et al.*, 2020). Most of this cleaning procedure had been

automated and was PC-operated using LabView™. After cleaning the sample gas, it was transferred into a cold trap with 5 Å molecular sieve beads, using a He stream at a flowrate of 10 mL min^{-1}. After He was evacuated from this trap, the sample was expanded into a bellow of a ThermoFinnigan™ MAT253 gas source mass spectrometer by heating the trap in a water bath at 50 °C. The $\delta^{17}O$ and $\delta^{18}O$ values of the samples were then determined by measuring O_2^+ ions at m/z = 32, 33, and 34 for ~40 minutes relative to a reference gas that was calibrated against the VSMOW2 and SLAP2 water standards (Pack *et al.*, 2016).

The triple oxygen isotope compositions of the samples are reported here relative to the composition of San Carlos olivine. Analytical sessions typically comprised measurements of eight samples that were bracketed by a total of six measurements of San Carlos olivine for each individual session. Two different fractions of San Carlos olivine were used for bracketing throughout the course of this study. These two fractions have identical $\Delta'^{17}O$ values at the level of <1 ppm, but have apparently different $\delta^{18}O$ values: One fraction (Göttingen internal ID: 0215M) has a long-term $\delta^{18}O$ value of 5.18 ± 0.01 ‰ (n = 52) whereas the other fraction (Göttingen internal ID: 0919) has a long-term $\delta^{18}O$ value 5.34 ± 0.01 ‰ (n = 91) relative to the composition of UWG-2 garnet ($\delta^{18}O$ = 5.74 ‰; Valley *et al.*, 1995). The samples were normalised to the $\Delta'^{17}O$ value of San Carlos olivine of −51.8 ppm, which is the average value for San Carlos olivine from the studies by Pack *et al.* (2016), Sharp *et al.* (2018), and Wostbrock *et al.* (2020).

S-3. Determining the Bulk Silicate Earth $\Delta'^{17}O$ Value

The $\Delta'^{17}O$ of the bulk silicate Earth (BSE) was previously determined by Herwartz *et al.* (2014; with data from Pack and Herwartz, 2014), Greenwood *et al.* (2018; with data from Starkey *et al.*, 2016), and Cano *et al.* (2020) with precisions of up to ca. 2–3 ppm (1 s.d.) relative to the composition of San Carlos olivine. Some of the samples that were included in these previous studies, however, possibly do not have representative $\Delta'^{17}O$ values for the BSE. Greenwood *et al.* (2018) and Cano *et al.* (2020) included in their studies a number

of glasses and phenocrysts from mid-ocean ridge basalts. However, mid-ocean ridge basalts contain on average 2 % oxygen from subducted, altered oceanic crust and sediments with $\delta^{18}O$ values of ~10.5 ‰ (Eiler *et al.*, 2000). The $\Delta'^{17}O$ values of high-$\delta^{18}O$ altered oceanic crust and sediments are several tens of ppm lower than fertile mantle peridotite (Sengupta and Pack, 2018), implying that the $\Delta'^{17}O$ values of MORB can potentially be lower than fertile mantle peridotite at the <5 ppm level. Greenwood *et al.* (2018) also included samples from ocean island basalts (OIBs) in their study that were later interpreted to possibly reflect a component of subducted, altered oceanic crust in the mantle sources of the OIB samples (Cao *et al.*, 2019). We propose here that olivine in fertile mantle peridotite is possibly a more representative sample type to determine the $\Delta'^{17}O$ of the BSE than mantle melts. Whereas olivine in mantle peridotite can potentially have exchanged oxygen isotopes with fluids and/or melts in the mantle, the oxygen isotope compositions of those fluids and/or melts would have been buffered by the oxygen isotope composition of mantle olivine (Mattey *et al.*, 1994; Chazot *et al.*, 1997). Indeed, there seems little variation in $\delta^{18}O_{ol}$ values of mantle peridotite, even if mantle peridotite samples are considered that experienced pervasive metasomatism (Mattey *et al.*, 1994; Chazot *et al.*, 1997; Regier *et al.*, 2018).

We focused in our study on the analysis of olivine for multiple reasons. First, in mantle peridotite samples, the oxygen isotope composition of olivine is expected to be less affected by possible processes of mantle metasomatism compared to ortho- and clinopyroxene (Perkins *et al.*, 2006), if any of such effects are present in mantle peridotite at all. In the Archean peridotite samples, we additionally focused on the analysis of hand-picked olivine grains to avoid incipient serpentinisation of the samples from obscuring the measured oxygen isotope compositions. Focusing on the triple oxygen isotopes compositions of olivine had the additional advantage that possible mineral-dependent effects during the analytical procedure (*e.g.*, Young *et al.*, 2016) or hypothesised mineral-specific crystal-chemical effects in $\Delta'^{17}O$ (Kohl *et al.*, 2017) do not affect the conclusions presented here.

S-4. Mass Balance Calculations for Missing Late Veneer

Whereas the precise oxygen isotopic values of the pre-late veneer mantle are unknown, they can be calculated from the suggested $\Delta'^{17}O$ value of the pre-late veneer mantle for an assumed composition of the late veneer. In $\delta^{17}O$ versus $\delta^{18}O$ space, the compositions of the pre-late veneer mantle, the bulk silicate Earth and late veneer plot, by definition, on a mixing line (Fig. S-1a). The slope *m* and intercept *i* of the mixing line can be calculated from the $\delta^{17}O$ and $\delta^{18}O$ values of the bulk silicate Earth (BSE) and late veneer (LV):

$$\delta^{17}O = m\delta^{18}O + i \qquad \text{(Eq. S-1a)}$$

with:

$$m = \frac{\delta^{17}O_{LV} - \delta^{17}O_{BSE}}{\delta^{18}O_{LV} - \delta^{18}O_{BSE}} \qquad \text{(Eq. S-1b)}$$

and

$$i = \delta^{17}O_{LV} - m\,\delta^{18}O_{LV} \qquad \text{(Eq. S-1c)}$$

In linearised triple oxygen isotope space, the pre-late veneer mantle also plots on a line with slope 0.528 and intercept that equals the $\Delta'^{17}O$ of the pre-late veneer mantle (PLVM), in per-mil (Fig. S-1b):

$$1000 \ln\left(\frac{\delta^{17}O}{1000} + 1\right) = 0.528 \times 1000 \ln\left(\frac{\delta^{18}O}{1000} + 1\right) + \frac{\Delta'^{17}O_{PLVM}}{1000} \qquad \text{(Eq. S-2)}$$

The δ values of the pre-late veneer mantle correspond to the point of intersection of these two relations (Fig. S-1), i.e.:

$$0.528\delta'^{18}O_{PLVM} + \frac{\Delta'^{17}O_{PLVM}}{1000} = 1000ln\left[m\, e^{\frac{\delta'^{18}O_{PLVM}}{1000}} - m + \frac{i}{1000} + 1\right] \qquad \text{(Eq. S-3)}$$

Eq. (S-3) cannot be solved algebraically, as it has a linear term on the left versus a logarithmic term on the right side, respectively. Instead, the $\delta'^{18}O$ values of the PLVM can be approximated from Eq. (S-3) using the Newton-Raphson method:

$$\delta'^{18}O_{n+1} = \delta'^{18}O_n - \frac{f_{(\delta'^{18}O_n)}}{f'_{(\delta'^{18}O_n)}} \quad \text{(Eq. S-4)}$$

The $\delta'^{18}O_{PLVM}$ value can be used to determine $\delta^{18}O_{PLVM}$, which in turn allows to calculate the missing oxygen atom fraction from the pre-late veneer mantle for an assumed composition of the late veneer. The missing oxygen atom fraction is given by:

$$f_{MLV} = \frac{\delta^{18}O_{BSE} - \delta^{18}O_{PLVM}}{\delta^{18}O_{LV} - \delta^{18}O_{PLVM}} \times \frac{[O]_{BSE}}{[O]_{LV}} \quad \text{(Eq. S-5)}$$

The concentration of oxygen in late accreted materials was assumed in this study to be similar to CI chondrites (46.5 wt. %), with the bulk silicate Earth having 44.33 wt. % oxygen (Palme and O'Neill, 2003). Missing late veneer is expressed in this study relative to the Earth's mass of 5.972×10^{24} kg, assuming a core mass fraction of 32.5 %.

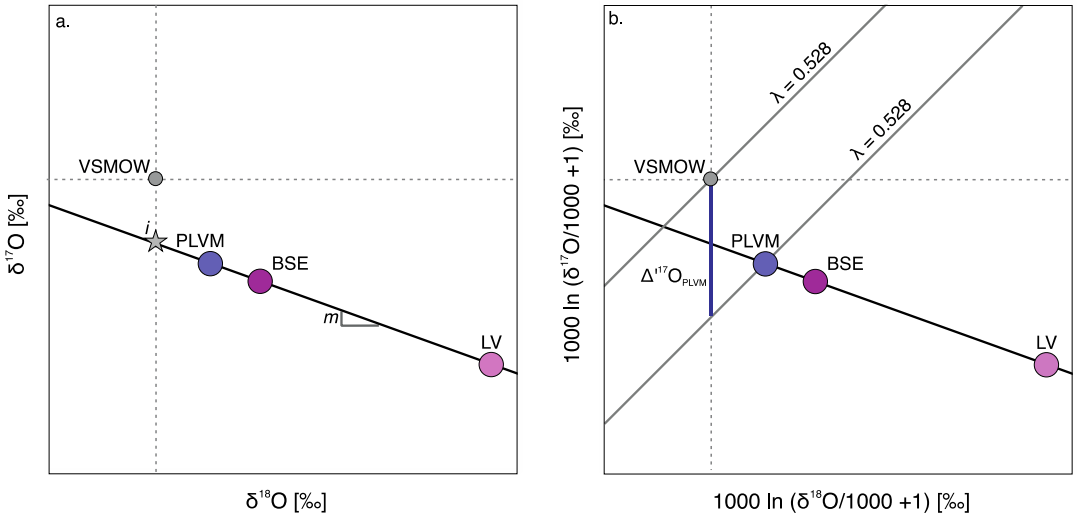

Figure S-1 **(a)** The triple oxygen isotope composition of the pre-late veneer mantle (PLVM) plots in $\delta^{17}O$ versus $\delta^{18}O$ space, by definition, on a mixing line with the compositions of the bulk silicate Earth (BSE) and late veneer (LV). The slope *m* and intercept *i* of the mixing line can be calculated from the triple oxygen isotope compositions of the bulk silicate Earth and an assumed composition for the late veneer (Eq. S-1). **(b)** The triple oxygen isotope composition of the pre-late veneer mantle plots by definition also on a line in $\delta'^{17}O$ versus $\delta'^{18}O$ space with slope $\lambda = 0.528$ and an intercept that equals the $\Delta'^{17}O$ value of the pre-late veneer mantle (Eq. S-2). The point of intersection of Eq. S-1a and Eq. S-2 gives the $\delta^{17}O$ and $\delta^{18}O$ values of the pre-late veneer mantle for an assumed composition of the late veneer.

Using Equations S-1 to S-5, we determined in a Monte Carlo simulation the possible mass of late veneer that can be missing from the early Archean mantle if the missing component had similar compositions to carbonaceous chondrite groups. All carbonaceous chondrite meteorites for which triple oxygen isotope data are available were considered as possible end members for the composition of the late veneer, *i.e.* f_{MLV} was calculated using the oxygen isotope composition of each single meteorite specimen for which data are available (Table S-3). The oxygen isotopic values of the BSE were sampled from a normally distributed data population with $\delta^{18}O = 5.41$ ‰ and $\Delta'^{17}O = -51.6 \pm 2.1$ (1 s.d.). The $\Delta'^{17}O$ value of the pre-late veneer mantle

was sampled from a normally distributed data population as well, using the mean value and standard deviation from this study ($\Delta'^{17}O = -52.3 \pm 1.7$ ppm; 1 s.d.). The 97.72nd percentile of the outcomes of the simulations are considered as the uppermost likely values for missing late veneer.

Supplementary Tables

Table S-1 Triple oxygen isotope compositions of olivine in post-Archean mantle peridotite[1].

Sample ID	Sample locality	Lithology	$\delta^{17}O$ [‰]	±	$\delta^{18}O$ [‰]	±	$\Delta'^{17}O$ [ppm]	±	*n*
Subcontinental lithospheric mantle peridotite									
15koz2	Kozákov volcano, northeast Bohemia (Czech Republic)	sp-lhz	2.73	0.03	5.28	0.06	−53	4	3
31631	Dreiser Weiher maar, Volcanic West Eifel (Germany)	sp-lhz	2.68	0.04	5.18	0.08	−50	4	3
3926-SC3	Hoher Hagen volcanic hill, Hessian graben (Germany)	sp-lhz	2.70	0.06	5.21	0.11	−50	4	3
SP15-VB	Gonterskirchen quarry, Vogelsberg volcanic field (Germany)	sp-lhz	2.68	0.05	5.18	0.09	−54	5	3
SP08-VB	Mont Briançon volcano, French Massif Central (France)	sp-lhz	2.73	0.03	5.27	0.06	−54	4	3
K-L6	Kilbourne hole maar, Potrillo volcanic field (Texas, USA)	sp-lhz	2.76	0.03	5.34	0.06	−52	4	3
8520-12	Atsagin-Dush volcano, Dariganga lava plateau (Mongolia)	sp-lhz	2.66	0.03	5.15	0.06	−53	3	6
TAA31c	Great Rift Valley (Ethiopia)	sp-lhz	2.70	0.03	5.22	0.06	−48	6	3
14MTM1	Tafraout Maar, Azrou volcanic field, Middle Atlas (Morocco)	sp-lhz	2.73	0.04	5.28	0.08	−49	5	2
WR21	Washington Ridge, Mount Melb. volcanic field (Antarctica)	sp-lhz	2.70	0.03	5.22	0.06	−52	4	5
08CL-009	Changle volcano, Shandong province (China)	sp-lhz	2.62	0.04	5.06	0.07	−50	6	2
Orogenic peridotite									
14BB2	Beni Boussera peridotite massif (Morocco)	dn	2.64	0.04	5.10	0.07	−52	5	2
Sub-oceanic lithospheric mantle peridotite									
SP16-LZ-01	Lanzarote, Canary Islands (Spain)	sp-lhz	2.70	0.03	5.21	0.07	−50	4	4
SP16-TF-01	Tenerife, Canary Islands (Spain)	sp-lhz	2.65	0.03	5.13	0.06	−52	4	3
ERG3-33a	Hualālai volcano, Island of Hawai'i (Hawaii, USA)	dn	2.76	0.03	5.34	0.05	−55	5	4
Post-Archean mantle peridotite (mean ± 1 s.d.)			**2.70**	**0.04**	**5.21**	**0.08**	**−51.6**	**2.1**	**15**

[1] $\Delta'^{17}O = 1000\,[\ln(\delta^{17}O/1000 + 1) - 0.528 \times (1000\,\ln(\delta^{18}O/1000 + 1)]$. Sample compositions are expressed relative to the composition of San Carlos olivine with $\Delta'^{17}O = -51.8$ ppm and $\delta^{18}O = 5.17$ ‰ or 5.33 ‰, depending on the San Carlos olivine fraction that was used for bracketing of the samples (see section S-2). Uncertainties for individual samples are given as ±1 s.e.m. for the indicated number n of analyses, whereas mean values are given with uncertainties of ±1 s.d. spl-lhz, spinel lherzolite; dn, dunite.

Table S-2 Triple oxygen isotope compositions of olivine in early Archean peridotite[1] (continues on next page).

Sample ID	Sample locality	Lithology	$\delta^{17}O$ [‰]	±	$\delta^{18}O$ [‰]	±	$\Delta'^{17}O$ [ppm]	±	*n*
Peridotite enclaves in the Itsaq Gneiss Complex (3.8–3.7 Ga)									
194855B	Isua Supracrustal Belt	dn	2.45	0.04	4.74	0.07	−51	5	2
194859	Isua Supracrustal Belt	dn	2.33	0.04	4.52	0.07	−56	5	2
194861	Isua Supracrustal Belt	dn	2.47	0.04	4.79	0.07	−53	5	2
194887A	Isua Supracrustal Belt	dn	2.33	0.04	4.51	0.07	−49	5	2
10-27	South of Isua Supracrustal Belt	dn	2.20	0.04	4.27	0.07	−50	5	2
10-28	South of Isua Supracrustal Belt	dn	2.26	0.03	4.38	0.06	−47	4	3
10-09	Narssaq ultramafic body	dn	1.44	0.03	2.81	0.06	−45	4	3
205065	Narssaq ultramafic body	dn	2.08	0.04	4.05	0.07	−51	8	2
208319	Narssaq ultramafic body	dn	2.24	0.04	4.33	0.07	−46	5	2
479902	Ujaragssuit Nunât	dn	2.46	0.03	4.77	0.06	−50	4	3
479903	Ujaragssuit Nunât	dn	2.34	0.04	4.54	0.07	−52	8	2
479904	Ujaragssuit Nunât	dn	2.69	0.07	5.20	0.13	−54	4	3
479908	Ujaragssuit Nunât	dn	3.19	0.04	6.15	0.07	−48	5	2
479909	Ujaragssuit Nunât	dn	3.23	0.03	6.24	0.06	−59	4	3
479919	Ujaragssuit Nunât	dn	2.50	0.11	4.85	0.21	−51	5	3
479929	Ujaragssuit Nunât	dn	2.51	0.04	4.85	0.07	−47	5	2
479939	Ujaragssuit Nunât	dn	2.41	0.07	4.67	0.13	−52	3	6
Itsaq Gneiss Complex (mean ± 1 s.d.)			2.42	0.40	4.69	0.76	−50.6	3.5	

Table S-2 (continued) Triple oxygen isotope compositions of olivine in early Archean peridotite[1].

Sample ID	Sample locality	Lithology	$\delta^{17}O$ [‰]	±	$\delta^{18}O$ [‰]	±	$\Delta'^{17}O$ [ppm]	±	*n*
Peridotite enclaves in the Fiskefjord region (3.0 Ga)									
482006	Fiskefjord	dn	2.53	0.03	4.88	0.06	−50	4	3
482032	Fiskefjord	dn	2.47	0.03	4.78	0.06	−51	4	3
482033	Fiskefjord	dn	2.73	0.04	5.28	0.07	−49	5	2
482034	Fiskefjord	dn	2.72	0.05	5.25	0.09	−53	4	3
482041	Fiskefjord	dn	2.51	0.03	4.86	0.05	−53	7	4
482054	Fiskefjord	dn	2.43	0.04	4.71	0.07	−54	4	4
Fiskefjord region (mean ± 1 s.d.)			2.56	0.13	4.96	0.24	−51.8	2.0	6
Early Archean mantle (mean ± 1 s.d.)			**2.46**	**0.35**	**4.76**	**0.67**	**−50.9**	**3.2**	**23**
Early Archean mantle (extrapolated ± 1 s.d. to $\delta^{18}O$ = 5.21 ‰)			**2.70**	**0.06**	**5.21**	**0.08**	**−52.3**	**1.7**	**23**

[1] $\Delta'^{17}O = 1000\,[\ln(\delta^{17}O/1000 + 1) - 0.528 \times (1000\ln(\delta^{18}O/1000 + 1)]$. Sample compositions are expressed relative to the composition of San Carlos olivine with $\Delta'^{17}O$ = −51.8 ppm and $\delta^{18}O$ = 5.17 ‰ or 5.33 ‰, depending on the San Carlos olivine fraction that was used for bracketing of the samples (see section S-2). Uncertainties for individual samples are given as ±1 s.e.m. for the indicated number of analyses *n*, whereas mean values are given with uncertainties of ±1 s.d. dn, dunite.

Table S-3 Triple oxygen isotope compositions of chondrites (compilation from the *Meteoritical Bulletin Database*).

Table S-3 is available for download (Excel file) at https://www.geochemicalperspectivesletters.org/article2120.

References

Bennett, V.C., Nutman, A.P., Esat, T.M. (2002) Constraints on mantle evolution from $^{187}Os/^{188}Os$ isotopic compositions of Archean ultramafic rocks from southern West Greenland (3.8 Ga) and Western Australia (3.46 Ga). *Geochimica et Cosmochimica Acta* 66, 2615–2630.

Cano, E.J., Sharp, Z.D., Shearer, C.K. (2020) Distinct oxygen isotope compositions of the Earth and Moon. *Nature Geoscience* 13, 270–274.

Cao, X., Bao, H., Gao, C., Liu, Y., Huang, F., Peng, Y., Zhang, Y. (2019) Triple oxygen isotope constraints on the origin of ocean island basalts. *Acta Geochimica* 38, 327–334.

Chazot, G., Lowry, D., Menzies, M., Mattey, D. (1997) Oxygen isotopic composition of hydrous and anhydrous mantle peridotites. *Geochimica et Cosmochimica Acta* 61, 161–169.

Dymek, R.F., Boak, J.L., Brothers, S.C. (1988) Titanian chondrodite and titanian clinohumite-bearing metadunite from the 3800 Ma Isua supracrustal belt, West Greenland; chemistry, petrology and origin. *American Mineralogist* 73, 547–558.

Eiler, J.M., Schiano, P., Kitchen, N., Stolper, E.M. (2000) Oxygen-isotope evidence for recycled crust in the sources of mid-ocean-ridge basalts. *Nature* 403, 530–534.

Fischer-Gödde, M., Elfers, B.M., Münker, C., Szilas, K., Maier, W.D., Messling, N., Morishita, T., Van Kranendonk, M., Smithies, H. (2020) Ruthenium isotope vestige of Earth's pre-late-veneer mantle preserved in Archaean rocks. *Nature* 579, 240–244.

Frei, R., Polat, A., Meibom, A. (2004) The Hadean upper mantle conundrum: Evidence for source depletion and enrichment from Sm-Nd, Re-Os, and Pb isotopic compositions in 3.71 Gy boninite-like metabasalts from the Isua Supracrustal Belt, Greenland. *Geochimica et Cosmochimica Acta* 68, 1645–1660.

Friend, C.R.L., Bennett, V.C., Nutman, A.P. (2002) Abyssal peridotites >3,800 Ma from southern West Greenland: Field relationships, petrography, geochronology, whole-rock and mineral chemistry of dunite and harzburgite inclusions in the Itsaq Gneiss Complex. *Contributions to Mineralogy and Petrology* 143, 71–92.

Friend, C.R.L., Nutman, A.P. (2011) Dunites from Isua, Greenland: A ca. 3720 Ma window into subcrustal metasomatism of depleted mantle. *Geology* 39, 663–666.

Greenwood, R.C., Barrat, J.A., Miller, M.F., Anand, M., Dauphas, N., Franchi, I.A., Sillard, P., Starkey, N.A. (2018) Oxygen isotopic evidence for accretion of Earth's water before a high-energy Moon-forming giant impact. *Science Advances* 4, 5928.

Herwartz, D., Pack, A., Friedrichs, B., Bischoff, A. (2014) Identification of the giant impactor Theia in lunar rocks. *Science* 344, 1146–1150.

Kohl, I.E., Warren, P.H., Schauble, E.A., Young, E.D. (2017) Limitations on $\Delta'^{17}O$ as a tracer of provenance revealed by mineral specific values from lunar and terrestrial anorthosites. *Lunar and Planetary Science Conference No. 1964*, 2292.

Lowry, D., Appel, P.W.U., Rollinson, H.R. (2003) Oxygen isotopes of an Early Archaean layered ultramafic body, southern West Greenland: Implications for magma source and post-intrusion history. *Precambrian Research* 126, 273–288.

Mattey, D., Lowry, D., Macpherson, C. (1994) Oxygen isotope composition of mantle peridotite. *Earth and Planetary Science Letters* 128, 231–241.

Nishio, I., Morishita, T., Szilas, K., Pearson, G., Tani, K.I., Tamura, A., Harigane, Y., Guotana, J.M. (2019) Titanian clinohumite-bearing peridotite from the ulamertoq ultramafic body in the 3.0 Ga akia terrane of southern west Greenland. *Geosciences (Switzerland)* 9, 153.

Nutman, A.P., Friend, C.R.L., Horie, K., Hidaka, H. (2007) Chapter 3.3 The Itsaq Gneiss Complex of

Southern West Greenland and the Construction of Eoarchaean Crust at Convergent Plate Boundaries. In: van Kranendonk, M.J., Smithies, R.H., Bennett, V.C. (Eds.) *Developments in Precambrian Geology 15: Earth's Oldest Rocks*. Elsevier, Amsterdam, 187–218.

Nutman, A.P., McGregor, V.R., Friend, C.R.L., Bennett, V.C., Kinny, P.D. (1996) The Itsaq Gneiss Complex of southern West Greenland; the world's most extensive record of early crustal evolution (3900–3600 Ma). *Precambrian Research* 78, 1–39.

Pack, A., Herwartz, D. (2014) The triple oxygen isotope composition of the Earth mantle and understanding $\Delta^{17}O$ variations in terrestrial rocks and minerals. *Earth and Planetary Science Letters* 390, 138–145.

Pack, A., Tanaka, R., Hering, M., Sengupta, S., Peters, S., Nakamura, E. (2016) The oxygen isotope composition of San Carlos olivine on the VSMOW2-SLAP2 scale. *Rapid Communications in Mass Spectrometry* 30, 1495–1504.

Palme, H., O'Neill, H. (2003) 2.01 – Cosmochemical estimates of mantle composition. In: Holland, H.D., Turekian, K.K. (Eds.) *Treatise on Geochemistry*. First Edition, Elsevier, Oxford. 1–38..

Perkins, G.B., Sharp, Z.D., Selverstone, J. (2006) Oxygen isotope evidence for subduction and rift-related mantle metasomatism beneath the Colorado Plateau-Rio Grande rift transition. *Contributions to Mineralogy and Petrology* 151, 633.

Peters, S.T.M., Szilas, K., Sengupta, S., Kirkland, C.L., Garbe-Schönberg, D., Pack, A. (2020) >2.7 Ga metamorphic peridotites from southeast Greenland record the oxygen isotope composition of Archean seawater. *Earth and Planetary Science Letters* 544, 116331.

Regier, M.E., Miškovi, A., Ickert, R.B., Pearson, D.G., Stachel, T., Stern, R.A., Kopylova, M. (2018) An oxygen isotope test for the origin of Archean mantle roots. *Geochemical Perspectives Letters* 9, 6–10.

Rollinson, H. (2002) A Metamorphosed, Early Archaean Chromitite from West Greenland: Implications for the Genesis of Archaean Anorthositic Chromitites. *Journal of Petrology* 43, 2143–2170.

Rollinson, H. (2007) Recognising early Archaean mantle: A reappraisal. *Contributions to Mineralogy and Petrology* 154, 241–252.

Sengupta, S., Pack, A. (2018) Triple oxygen isotope mass balance for the Earth's oceans with application to Archean cherts. *Chemical Geology* 495, 18–26.

Sharp, Z.D., Wostbrock, J.A.G., Pack, A. (2018) Mass-dependent triple oxygen isotope variations in terrestrial materials. *Geochemical Perspectives Letters* 7, 27–31.

Starkey, N.A., Jackson, C.R.M., Greenwood, R.C., Parman, S., Franchi, I.A., Jackson, M., Fitton, J.G., Stuart, F.M., Kurz, M., Larson, L.M. (2016) Triple oxygen isotopic composition of the high-$^{3}He/^{4}He$ mantle. *Geochimica et Cosmochimica Acta* 176, 227–238.

Szilas, K., Kelemen, P.B., Bernstein, S. (2015a) Peridotite enclaves hosted by Mesoarchaean TTG-suite orthogneisses in the Fiskefjord region of southern West Greenland. *GeoResJ* 7, 22–34.

Szilas, K., Kelemen, P.B., Rosing, M.T. (2015b) The petrogenesis of ultramafic rocks in the 3.7 Ga Isua supracrustal belt, southern West Greenland: Geochemical evidence for two distinct magmatic cumulate trends. *Gondwana Research* 28, 565–580.

Valley, J.W., Kitchen, N., Kohn, M.J., Niendorf, C.R., Spicuzza, M.J. (1995) UWG-2, a garnet standard for oxygen isotope ratios: Strategies for high precision and accuracy with laser heating. *Geochimica et Cosmochimica Acta* 59, 5223–5231.

van de Löcht, J. (2019) *Geochemistry and petrology of ~3.8 Ga mafic-ultramafic enclaves in the Itsaq Gneiss Complex, SW Greenland*. PhD thesis, Universität zu Köln, 208 pp.

van de Löcht, J., Hoffmann, J.E., Li, C., Wang, Z., Becker, H., Rosing, M.T., Kleinschrodt, R., Münker, C. (2018) Earth's oldest mantle peridotites show entire record of late accretion. *Geology* 46, 199–202.

van de Löcht, J., Hoffmann, J.E., Rosing, M.T., Sprung, P., Münker, C. (2020) Preservation of Eoarchean

mantle processes in ~3.8 Ga peridotite enclaves in the Itsaq Gneiss Complex, southern West Greenland. *Geochimica et Cosmochimica Acta* 280, 1–25.

Wiechert, U., Ionov, D.A., Wedepohl, K.H. (1997) Spinel peridotite xenoliths from the Atsagin-Dush volcano, Dariganga lava plateau, Mongolia: A record of partial melting and cryptic metasomatism in the upper mantle. *Contributions to Mineralogy and Petrology* 126, 345–364.

Wostbrock, J.A.G., Cano, E.J., Sharp, Z.D. (2020) An internally consistent triple oxygen isotope calibration of standards for silicates, carbonates and air relative to VSMOW2 and SLAP2. *Chemical Geology* 533, 119432.

Young, E.D., Kohl, I.E., Warren, P.H., Rubie, D.C., Jacobson, S.A., Morbidelli, A. (2016) Oxygen isotopic evidence for vigorous mixing during the Moon-forming giant impact. *Science* 351, 493–496.